Article:

1 **Pyrolysis of plastic wastes in a fountain confined conical spouted bed**

2 **reactor: determination of stable operating conditions**

3 Santiago Orozco[a], Jon Alvarez[b]*, Gartzen Lopez[a,c], Maite Artetxe[a], Javier Bilbao[a] and

4 Martin Olazar[a]

5 [a]Department of Chemical Engineering, University of the Basque Country UPV/EHU,

6 P.O. Box 644-E48080 Bilbao, Spain

7 [b]Department of Chemical and Environmental Engineering, University of the Basque

8 Country UPV/EHU, Nieves Cano 12, 01006 Vitoria-Gasteiz, Spain.

9 [c]IKERBASQUE, Basque Foundation for Science, Bilbao, Spain

10 *To whom correspondence should be addressed. Telephone: +34946012527. Fax: +34

11 946 013 500. E-mail: jon.alvarezg@ehu.es.

12 **Abstract**

13 The performance of both fluidized and spouted bed reactors in the pyrolysis of waste

14 plastics is conditioned by particle agglomeration phenomena, which worsen the quality

15 of the gas-solid contact and eventually lead to defluidization. The objective of this work

16 is to determine the optimum conditions for stable operation (without defluidization) in a

17 bench scale plant fitted with a fountain confined conical spouted bed reactor and

18 equipped with a nonporous draft tube, which operates in continuous mode. The

19 insertion of these devices enhances the gas-solid contact, especially in the fountain

20 region, and leads to a highly stable hydrodynamic regime, with these features being of

21 especial relevance for the *in situ* catalytic pyrolysis of waste plastics. This paper deals

22 with the effect different variables have on the minimum temperature for stable operation

23 by avoiding defluidization. The variables analyzed are as follows: plastic type (HDPE,

LDPE, PP, PS, PET and PMMA), plastic feed rate, mass of inert material in the bed, spouting velocity and use of catalyst. The results show that polymers whose chains decompose at low temperatures or have high degrees of branching require low operating temperatures. Besides, as the ratio of bed mass to plastic feed rate ($W_{bed}/Q_{plastic}$) and/or spouting velocity were increased, the temperature required to avoid defluidization was also reduced. The use of a catalyst also reduced the temperature required for stable operation, as the activation energy of cracking reactions is greatly reduced, and so reaction rate is increased.

Keywords: defluidization, plastic waste, pyrolysis, conical spouted bed, fountain confinement

1. Introduction

The growing plastic waste accumulation together with its low degradability have boosted the global concern about the need of suitable management strategies due to the serious environmental problems caused by this waste, especially in marine environments [1, 2]. In the European Union (EU), more than 30 % of the plastics are still disposed in landfills and, although this percentage is slowly decreasing, its current situation is far from being satisfactory [3]. Moreover, uncontrolled incineration of waste plastics also leads to environmental concerns due to the release of dioxins, furans, mercury and polychlorinated biphenyls [4]. Hence, new efficient and environmentally friendly processes are being developed for plastic valorization, with thermal and catalytic pyrolysis being two of the most feasible methods for large scale implementation [5-8].

Different types of reactors (at lab and pilot scale) operating in batch, semi-batch and continuous-flow mode have been used in the pyrolysis of plastics, as are fluidized beds (FBR) [9], conical spouted beds (CSBR) [10], fixed beds [11], rotary kilns [12, 13], auger reactors [14] and microwave assisted reactors [15]. Among these technologies, FBRs and CSBRs have been successfully applied in the pyrolysis of waste solids due to their gas-solid contact features [16, 17]. Indeed, energy supply is the major difficulty in the pyrolysis of plastics due to their poor thermal conductivity [18], and fluidized and conical spouted beds ensure high heat and mass transfer rates between phases, leading to bed isothermicity. Nevertheless, operation at large scale in these reactors is compromised by particle agglomeration phenomenom, which worsens the quality of fluidization and eventually leads to defluidization [19, 20]. The agglomeration in gas-solid contactors during plastic pyrolysis is caused by a "coating-induced" mechanism, in which a sticky layer is formed on the surface of the particles due to the adhesive

3

nature of plastics when they are heated at high temperature [21]. The tendency of the particles to agglomerate will depend on their stickiness, momentum and surface contact [20]. Particle agglomeration generally begins with the formation of small agglomerates of bed material, which may increase and lead to bed collapse. At the initial stage, the external surface of the plastic particles fed into the reactor is softened, but its core is still cold (consequence of the poor thermal conductivity) [22]. The softened surface becomes adhesive and forms agglomerates made up of a plastic particles surrounded by sand ones. When the entire plastic particle is softened, its material is distributed by coating the surrounding sand particles, which will fuse together if the thickness of their coating layer is higher than a critical value. The mechanism for the formation of these agglomerates is different depending on the type of polymer, and their growth may be attenuated or enhanced depending on the process parameters, such as plastic feed rate, bed mass and size of the inert solid particle [23-25]. Finally, when defluidization occurs a single large agglomerate appears in the upper zone of the stagnant bed (the plastic is fed from the top side) [26].

The procedure for avoiding defluidization in fluidized beds lies in minimizing the thickness of the fused plastic that coats the inert solid (sand), and can only be attained by increasing the sand/plastic ratio in the bed. This means that large amounts of sand are required to promote fluidization, which involves large reactor volumes and high gas flow rates and energy requirements, thereby decreasing the process yield [27]. The conical spouted bed reactor is an alternative to fluidized beds and its characteristics (vigorous particle movement and great gas flow rate versatility) make it is especially suitable for avoiding agglomeration problems in the pyrolysis of plastics, even when the operation is carried out under the conditions of maximum stickiness [27-28]. Figure 1 shows the vigorous solid circulation in a conventional CSBR, which allows operating

85   under isothermal conditions with almost perfect mixing for the solid and high heat and

86   mass transfer rates. This vigorous cyclic movement of sand particles allows for their

87   uniform coating with fused plastic and provides enough energy to the colliding particles

88   to avoid their agglomeration. Furthermore, the critical thickness of the layer that coats

89   the particles is an order of magnitude higher than that corresponding to the fluidized

90   bed, thus leading to higher yields by reactor volume unit. Apart from these facts, this

91   reactor has a simple design (distributor plate is not required) and requires lower

92   volumes than fluidized beds for the same capacity, simplifying the scaling up of the

93   pyrolysis process. However, a mixture containing coarse (plastic) and fine (sand and/or

94   catalysts) particles requires high gas velocities due to the coarse particles, and this

95   situation leads to fine particle entrainment [29]. The insertion of draft tubes is the only

96   way to attain stable spouting with relatively low gas velocities, but these devices with

97   fine particles lead to very high fountains, and therefore to severe elutriation [30, 31].

98   Different draft tube configurations are reported in the literature: conventional nonporous

99   draft tubes, porous draft tubes, and open-sided draft tubes [32]. The selection of a non-

100 porous draft tube involves operational advantages compared to porous and open sided

101 tubes, i.e., it allows for operating with lower gas flow rates and pressure drops [31, 32].

102 These features, especially the low gas flow rate requirement, is of great interest for

103 waste plastics pyrolysis. Moreover, the hydrodynamic regime attained operating with a

104 combination of non-porous draft tube and a fountain confiner has demonstrated high

105 catalysts efficiency in biomass gasification due to the improvement of the gas-solid

106 contact [33].

107

108
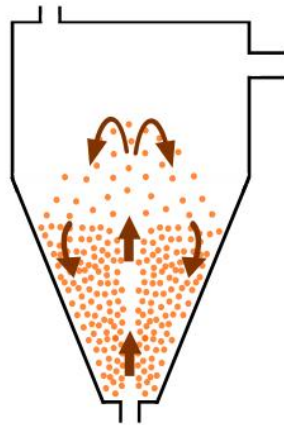
Figure 1. Diagrammatic representation of a conventional conical spouted bed.

110 The insertion of a fountain confiner in the reactor was proposed in order to improve the

111 CSBR hydrodynamic performance and avoid the elutriation of fine particles, [29]. This

112 simple device is a tube welded to the lid of the reactor and placed above the bed in order

113 to collect the particles from the spout. This device allows operating with much finer

114 particles than in conventional conical spouted beds, and therefore the gas flow rate for

115 spouting is considerably reduced. Moreover, the trajectory of the gas is also modified,

116 as it rises though the core of the fountain to its top. It then descends along the fountain

117 periphery (close to the confiner wall), and finally crosses the gap between the device

118 and the upper surface of the bed to rise along the annular zone between the confiner and

119 the contactor wall [34]. These modifications in the reactor hydrodynamics improve the

120 overall gas-solid contact in the bed and allow controlling the gas residence time.

121 Furthermore, these two properties confer an additional advantage upon the CSBR in

122 catalytic processes for waste valorization, since they promote the desired cracking

123 reactions [33]. Accordingly, the combination of both fountain confiner and draft tube

124 enhances the gas-solid contact in the fountain region and minimizes particle

125 entrainment, at the same time as it leads to a highly stable bed with hardly any effect on

126 the operating pressure drop. Thus, the insertion of these devices improved significantly

127 the CSBR performance in biomass steam gasification [33] and allowed stable operation

128 in the pyrolysis of microalgae, whose peculiar features (very light and fine particles)

129 lead to elutriation in conventional spouted beds [35]. Figure 2 shows a scheme of the

130 CSBR with the confined fountain and a non-porous draft tube. The trajectories of the

131 gas and the solid have been highlighted in both the entire bed and the surrounding of the

132 draft tube (enlarged zone). Furthermore, the initial formation of polymer-sand

133 aggregates is shown, i.e., when the melted plastic coats the sand particles. As previously

134 stated, as pyrolysis progresses these agglomerates may grow by their fusion with

135 surrounding particles, thus worsening fluidization quality.
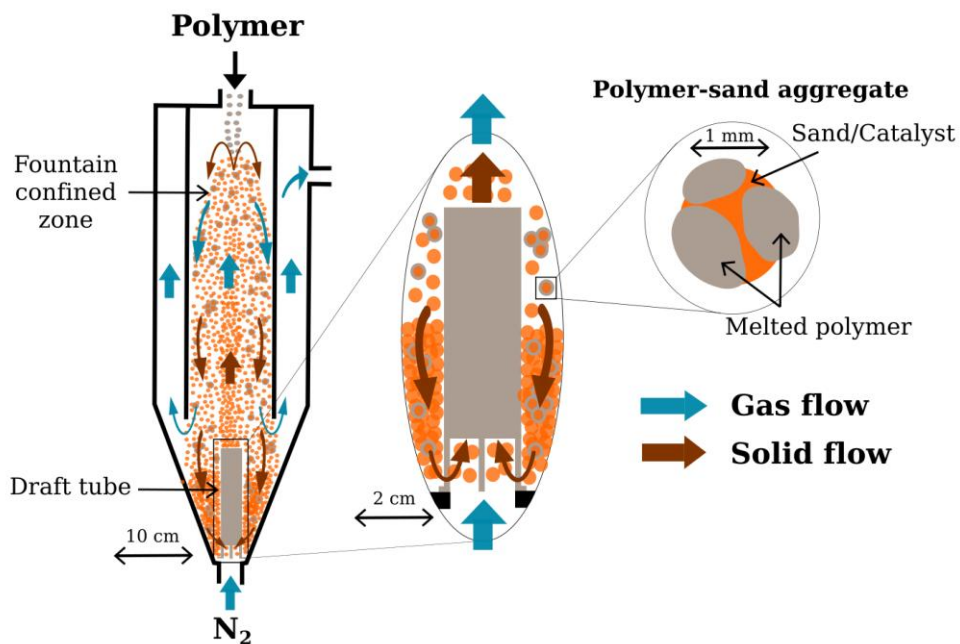
136
137 **Figure 2**. Gas and solid flow circulation in a fountain confined CSBR provided with a

138 non-porous drat tube during plastic pyrolysis.

139 This work addresses the pyrolysis of plastics in a bench scale unit provided with a

140 fountain confined CSBR operating in continuous mode. The main scope is to determine
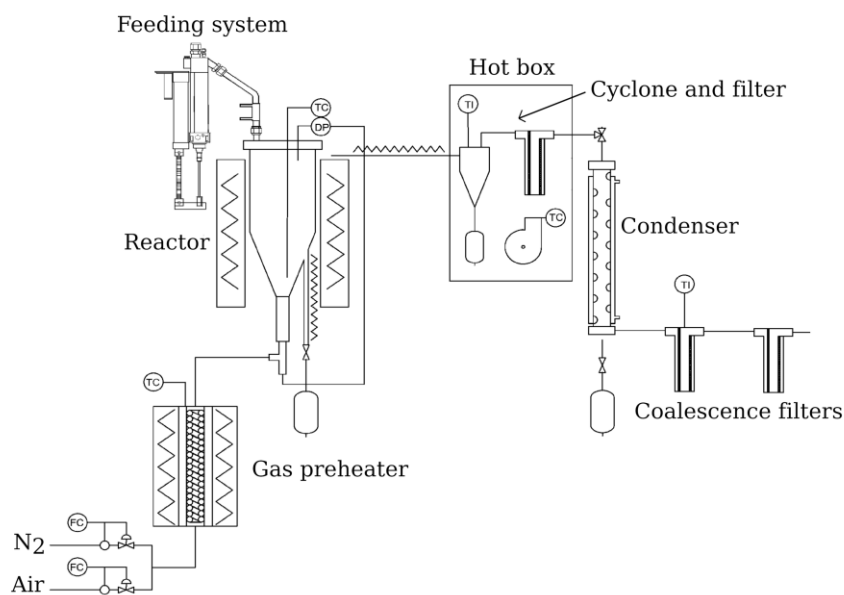
141 the minimum temperature for stable operation (at which bed defluidization is avoided)

142 under different operating variables. The parameters evaluated affecting fluidization

143 quality are as follows: plastic type and its feed rate, bed mass and minimum spouting

144 velocity. Moreover, the influence of using a catalyst was also analyzed, as the main

145 interest of this novel reactor lies in the improvement of the contact and efficiency in

146 catalytic processes for biomass and waste conversion.

2. Material and Methods

2.1. Experimental equipment

149 The experiments were conducted in a CSBR system provided with a fountain confiner

150 and a non-porous draft tube, which allow widening the operation range and improve the

151 hydrodynamic behavior of the reactor. The scheme of the bench scale plant used for

152 plastic pyrolysis is shown in Figure 3. The continuous pyrolysis unit with the fountain

153 confiner and the draft tube has been set-up and fine-tuned based on the knowledge

154 acquired in previous hydrodynamic studies in a cold unit [29, 34], a biomass

155 gasification unit [33, 36-38] and a microalgae pyrolysis unit operating in fountain

156 enhanced regime [35]. Furthermore, the CSBR technology with neither internal devices

157 nor fountain confiner has been satisfactorily applied in the pyrolysis and gasification of

158 different waste materials, such as waste tyres, plastics and different types of biomasses

159 [39-44].

160 The plant consists of the following elements: (i) solid feeding device (ii) gas feeding

161 device, (iii) pyrolysis reactor provided with a non-porous draft tube and fountain

162 confiner, (iv) high efficiency cyclone followed by sintered steel filter for retaining the

163 fine particles elutriated from the reactor and (v) a volatile condensation device.

Feeding system

Hot box

Cyclone and filter

Reactor

Condenser

Coalescence filters

Gas preheater

N₂

Air

164

Figure 3. Scheme of the bench scale plant equipped with a conical spouted reactor.

The solid feeding system consists of a vessel equipped with a vertical shaft connected to a piston placed below the bed of plastics, allowing their continuous feed when the piston rises. Besides, this device has also a vibrator that helps plastics feed into the reactor. In order to avoid plastics melting prior to entering the reactor and so avoid clogging of the device for their feeding, a shell pipe cooled by tap water has been inserted at the reactor inlet. Note that solid feeding compartment is watertight and the gas stream fully exits through the established sideway. The nitrogen flow rate is controlled by a mass flow meter, which allows feeding up to 30 L min^{-1}, and is heated to the reaction temperature by means of a preheater.

The plant's main device is the CSBR made of stainless steel and its main characteristics are shown in Figure 4. The total height of the reactor is 34 cm, the height of the conical section 20.5 cm, and the angle of the conical section 28∘. The diameter of the cylindrical

9

178 section is 12.3 cm, the bottom diameter 2 cm and the gas inlet diameter 1 cm. The

179 fountain confiner is an 8 cm diameter tube welded to the lid of the reactor that has the

180 lower end of the tube close to the surface of the bed, with its total length being 8.2 cm.

181 Finally, the draft tube is 1 cm in diameter and the height of entrainment zone is 2.5 cm.

182 Thus, this reactor can operate from the regime of spouted bed to vigorous fountain

183 enhanced one, in which a significant fraction of the bed is in the fountain, with low

184 nitrogen flow rates, ensuring a stable spouting. More detailed information about the

185 design and performance of the fountain confiner and the draft tubes within the CSBR

186 technology can be found elsewhere [33, 36, 45]. Moreover, the pyrolysis temperature

187 was measured and recorded by means of two K-type thermocouples located inside the

188 reactor, one in the annulus zone in direct contact with the bed and the other one close to

189 the wall. A pressure drop gauge was also installed and pressure measurements were

190 carried out by means of two taps inserted into the reactor input and output. Continuous

191 monitoring of temperature and pressure drop provided relevant information about the

192 quality of the spouting and allowed detecting defluidization [46].
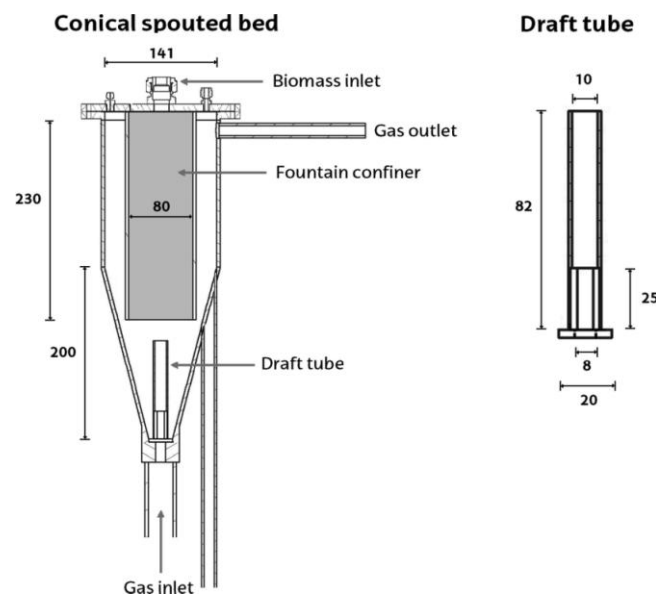
193

194 **Figure 4.** Dimensions of the reactor, fountain confiner and the non-porous draft tube.

In order to retain the fine solids elutriated from the reactor, the gaseous stream leaving the reactor was passed through a high-efficiency cyclone and a 25 µm sintered steel filter, both located in a hot box whose temperature was kept at 300 ºC. This temperature is enough to avoid coking problems and avoid the formation of carbonaceous residues. Then, the gases exiting the particle retention system crossed the condensation section consisting of a double shell tube condenser and a 60 µm stainless steel filter, both cooled by tap water.

2.2. Materials

The plastics used in this study were High and Low Density Polyethylene (HDPE and LDPE), polypropylene (PP), polystyrene (PS), Poly(ethylene terephthalate) (PET) and Poly(methyl methacrylate) (PMMA). HDPE, LDPE, PP and PS was supplied by *Dow Chemical* (Tarragona), PET by *Artenius PET Brand Seda Group* (Barcelona) and PMMA by *Altuglas International Arkema Group*. Given that no size reduction is required in the CSBR, the plastics were directly fed into the reactor in the form of pellets (4 mm). The main properties of these plastics are shown in Table 1. Unfortunately, the supplier did not provide the detailed composition of PMMA.

Table 1. Characteristics of the plastics used.

	HDPE	LDPE	PP	PS	PET	PMMA
Molecular weight ($kg\,mol^{-1}$)	46.2	92.2	50–90	311.6	25–30	120
Polydispersity	2.89	5.13	2.0	2.39	2.0	n.p
HHV ($MJ\,kg^{-1}$)	43	43	44	40	24	n.p
Ultimate analysis (wt%)						
C	85.7	85.7	85.7	92.3	62.5	60.0
H	14.3	14.3	14.3	7.7	4.2	8.0
O	-	-	-	-	33.3	32.0

n.p: not provided

213 Moreover, fountain confined conical spouted beds allow operating *in situ* with finer

214 catalyst particles than conventional conical spouted beds, which allows studying the

215 effect of commercial catalysts used in fluidized beds. Previous studies in a CSBR

216 showed that a spent Fluid Catalytic Cracking (FCC) catalyst had a very good

217 performance in the waste polyolefin cracking [47]. The selection of the catalysts used in

218 this study was based on its suitable activity and because it is easily available. In fact, the

219 spent FCC catalyst is an industrial residue that can be reutilized in the valorization of

220 waste plastics. Therefore, a spent FCC catalyst (supplied by Petronor) based on a zeolite

221 active phase was used in the catalytic pyrolysis of waste plastics. The catalyst particles

222 were sieved in order to use a size in the 90–150 μm range. The porous structure of the

223 catalyst was characterized by N_2 adsorption–desorption (Micromeritics ASAP 2010)

224 and the values of total acidity and average acid strength were obtained by simultaneous

225 monitoring of the differential adsorption of NH_3 at 150 °C by calorimetry and

226 thermogravimetry in a Setaram TG-DSC 111 equipment. Table 2 shows the main

227 properties of the spent FCC catalyst used in this study.

228 **Table 2**. Properties of the equilibrated FCC catalyst.

BET surface area ($m^2\ g^{-1}$)	143
Micropore surface area ($m^2\ g^{-1}$)	103
Mesopore volume ($cm^3\ g^{-1}$)	0,04
Average pore diameter (Å)	101
Acid strength ($kJ\ mmol\ NH_3^{-1}$)	105
Total acidity ($\mu mol\ NH_3\ g\ cat^{-1}$)	124

229

230 *2.3. Experimental procedure*

231 The effect of plastic type, plastic feed rate, bed mass, spouting velocity and use of

232 catalyst were studied in order to establish in each case the minimum temperature to

233   ensure stable operation avoiding bed defluidization. Runs were carried out in the

234   spouted bed provided with fountain confiner by varying plastic type (HDPE, LDPE, PP,

235   PS, PET and PMMA), bed mass (100, 150 and 250 g), plastic feed rate (0.5, 1, 2 and 3 g

236   min^{-1}), spouting velocity (1.2, 1.6, 2 and 4 times the minimum spouting velocity) and

237   amount of catalyst (7, 15 and 30 g of FCC spent catalyst). The ratio of plastic feed rate

238   to bed mass, $W_{bed}/Q_{plastic}$ was also changed according to the criterion proposed by Arena

239   and Mallestone [20]. They suggested that this ratio is the relevant modulus to study the

240   influence of both parameters in the defluidization phenomenom.

241   The operating conditions used in each experiment to analyze the influence of the

242   aforementioned parameters are shown in Table 3. As observed, a *base case* was selected

243   to ascertain the effect of the different parameters on the fluidization quality. Thus, the

244   reactor was loaded with 150 g of sand with a particle size in the 0.2-0.3 mm range and

245   air was used as the fluidizing agent during the heating period. When the reactor reached

246   the desired temperature, air was replaced with nitrogen and its flow rate was fixed at 4

247   times the minimum spouting velocity, which corresponds to 10 L min^{-1}. It should be

248   noted that the minimum spouting velocity (u_{ms}) and the fountain enhanced spouting

249   velocity (u) were previously determined by direct observation under the conditions

250   studied. Then, 1 g min^{-1} of HDPE was fed continuously for 10 min (unless bed

251   defluidization occurred before). This time is enough to guarantee that stable operation is

252   attained under the operating conditions to study. Once the run was finished, the N_2

253   stream was substituted by air stream to burn the remaining polymeric material and so

254   proceed with the next experiment. All the operational parameters (type of plastic,

255    $W_{bed}/Q_{plastic}$, spouting velocity and space time when the catalyst was used) were

256   changed in the runs, with the operating procedure being as described above. All the runs

257   were repeated three times to ensure process reproducibility. Note that the minimum

258 temperature refers to the lowest temperature measured at which defluidization

259 phenomena is avoided during the continuous operation. This means that lower

260 temperatures lead to poor fluidization during continuous operation and eventually bed

261 collapse.

262 **Table 3**. Operating conditions in each run to analyze the effect of different parameters

263 on bed performance.

Parameters analyzed / Operating conditions	Base case	W_{bed} / $Q_{plastic}$					Plastic type	u/u_{ms}	Catalyst		
Plastic type	HDPE	HDPE					LDPE PP PS PET PMMA	HDPE	HDPE		
$Q_{plastic}$ (g min^{-1})	1	0.5	2	3	1	1	1	1	1		
Bed material	Sand	Sand					Sand	Sand	Sand + Catalyst		
Catalyst (g)	-	-					-	-	7	15	30
Sand (g)	150	150	150	150	250	100	150	150	143	135	120
u/u_{ms}	4	4					4	1.2 1.6 2	4		
Q_{msN2} (L min^{-1})	2.5	2.5	2.5	2.5	2.8	2	2.5	2.5	1.75		
Q_{N2} (L min^{-1})	10	10	10	10	11.2	8	10	3 4 5	7		

264

265 The fluidization quality, and therefore the bed state during the reaction was followed by

266 visual observation of the bed to confirm whether defluidization occurred or not, as well

267 as by monitoring temperature and pressure drop. The evolution of pressure drop and

268 temperature with time was proven an effective technique for detecting fluidization

269 worsening and the time at which the bed was definitively stagnant or defluidized [26,

270 46, 48]. The values of both temperature and pressure drop fluctuated slightly with time

271 when the bed was fluidizing well, but these fluctuations as well as the absolute pressure

272 drop progressively decreased when fluidization became worse and their values remained

273 steady when finally defluidization occurred. It is well known that defluidization leads to

274 a decrease in the total bed pressure drop because most of the fluidizing gas flows

275 through large channels when the bed is collapsed [49-51]. Although the monitoring of

276 only pressure drop may provide useful information about defluidization, Shabanian et

277 al. [49] concluded that this strategy is too sensitive to other process changes, which may

278 occasionally lead to false alarms. Furthermore, the monitoring of only temperature or

279 pressure signals does not ensure a reliable detection of defluidization due to the risk of

280 false positives and false negatives. Visual observation proves that the monitoring of

281 both variables provides reliable information about the fluidization state. Thus, the

282 reactor lid was removed to observe the bed at the end of each run, with the nitrogen

283 flow rate maintaining at the same value as in the operation. When defluidization

284 occurred, the solid particles were fused together in a static bed.

285 *2.4. Thermogravimetric analysis of the plastics*

286 The pyrolysis characteristics of the plastic samples were determined in a TGA Q500IR

287 thermogravimetric analyzer. Thus, this simple analysis provides relevant information of

288 their pyrolysis behavior, such as the temperature required for their complete

289 devolatilization and the degradation rate. 10 mg of plastic were loaded in the crucible

290 and subjected to a heating rate of 10 ºC/min from room temperature to 700 ºC using a

291 nitrogen flow rate of 50 mL/min. To ensure full carbonization of the sample, a

292 temperature of 700 ºC was maintained for 60 min. Moreover, additional experiments

293 were carried out to evaluate the influence FCC catalysts have on HDPE degradation.

294 Interestingly, TGA analysis is able to reproduce the contact between fused polymer and

295 the catalyst, and allows monitoring the formation of volatiles. The capability of the

296 catalysts for converting the fused polymer into volatile compounds is critical on the

297 defluidization process. Accordingly, runs were carried out in the TGA by loading 5 mg

298 of FCC catalyst together with 10 mg of HDPE plastic in the crucible. The experiments

299   were repeated twice for each plastic to guarantee the reproducibility of the results. The

300   deviations observed were below 2% in mass.

301   **3. Results and discussion**

302   Sets of runs were carried out in the CSBR in order to delimit the minimum temperature

303   for stable operation. In each set, the operating parameters were fixed at given values and

304   temperature was increased in the runs. When the bed was defluidized, air was

305   introduced to burn the polymer and prepare the equipment for a new run at higher

306   temperature. This procedure was repeated in each set until the temperature avoiding

307   defluidization was found under these conditions.

308   The effect of the different operating parameters on the minimum temperature for stable

309   operation was ascertain by comparing the results with those of the *base case*. This was

310   the run carried out by feeding 1 g min^{-1} of HDPE into a bed of 150 g of silica sand with

311   a particle size in the 0.2-0.3 mm range and a nitrogen flow rate of 10 L min^{-1} (4 times

312   that for minimum spouting). Under these conditions, the minimum temperature for

313   stable operation was 520 ºC. At lower temperatures, defluidization occurred due to the

314   very low degradation rate of the polymer and its subsequent accumulation in the bed.

315   **3.1. Effect of plastic type**

316   One of the factors of greater influence on bed defluidization is polymer type. Thus, the

317   minimum temperature for stable operation differs depending on the molecular structure

318   of the polymer, which directly affects the degradation mechanism and its physical

319   properties. Thus, polymers with high degree of branching decompose at low

320   temperatures, and therefore require low operating temperatures to avoid bed collapse.

321   Derivative thermogravimetric (DTG) curves for LDPE, HDPE, PP, PS, PET and

322   PMMA are shown in Figure 5, which provide information of the pyrolytic degradation

323   mechanism of each plastic. Besides, the minimum temperatures for stable operation

324   under the *base case* conditions are shown in Figure 6. It should be noted that, in certain

325   cases, stable pyrolysis temperature in the CSBR is slightly higher than the end

326   temperature of the material pyrolysis. This difference is due to the limitations of heat

327   transfer in the fused plastic and the differences in the performance of the pyrolysis

328   process in the thermobalance and in the bench scale reactor. In a thermobalance, the

329   heating rate is low (10 ºC/min), and the contact time at any temperature is therefore high

330   enough for plastic devolatilization, which allows completing the pyrolysis at lower

331   temperatures. Conversely, the heating rates in the CSBR are very high and the gas-solid

332   contact time is much lower compared to that in the TG. Therefore, slightly higher

333   temperatures are required to complete volatilization in the bench scale CSBR.

334
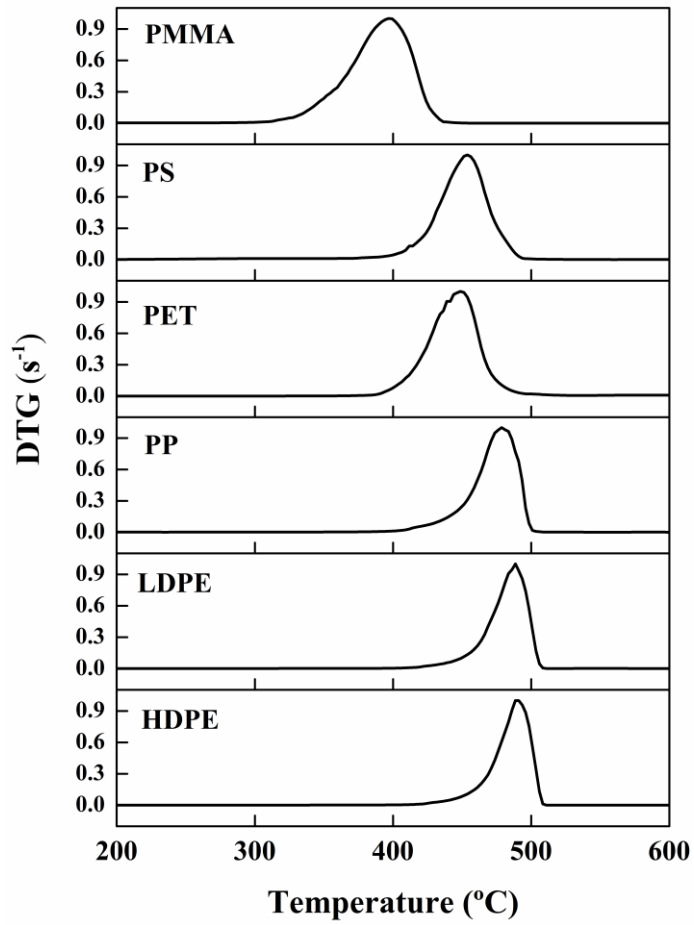
Figure 5. DTG curves for HDPE, LDPE, PP, PS, PET and PMMA.
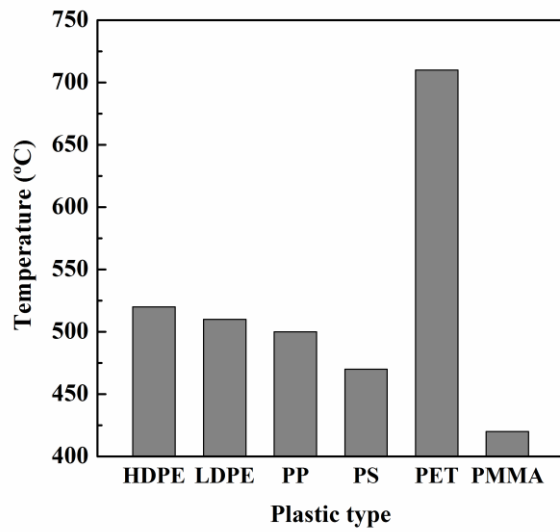
336

337 **Figure 6**. Minimum temperatures for stable operation in the fast pyrolysis of different

338 polymers. Operating conditions: plastic feed rate, 1 g min^{-1}; bed mass, 150 g; sand

339 particle size, 0.2-0.3 mm, and N$_2$ flow rate, 10 L min^{-1}.

340 As observed in Figure 6, PMMA followed by PS are the polymers that required the

341 lowest temperatures (420 and 470 ºC, respectively) under stable operating conditions in

342 the pyrolysis. In both cases, polymer degradation starts at lower temperatures than for

343 LDPE, HDPE and PP (Figure 5), and therefore thermal pyrolysis of PS and PMMA

344 occurred faster than in the case of polyolefins at the same reaction temperature [52].

345 Unlike polyolefins, PMMA and PS pyrolysis led to a high monomer recovery, i.e.,

346 methyl methacrylate (MMA) and styrene, respectively, since the reaction mechanism is

347 radical depolymerisation, in which the polymer chain is split by the action of heat [53-

348 56]. This type of reaction mechanism eases polymer degradation, accelerates reaction

349 rate and minimizes its accumulation in the bed, which allows operating at lower

350 pyrolysis temperatures.

351 Moreover, as observed in Figure 6, PP pyrolysis can be performed under stable

352 conditions at 500 ºC, followed by LDPE at 510 ºC and HDPE at 520 ºC. Despite the

353 similarity of polyolefin DTG curves shown in Figure 5, the degradation of PP starts and

354 finishes at slightly lower temperatures (390 and 500 ºC, respectively) compared to

355 HDPE and LDPE, thereby confirming they require lower temperatures to attain high

356 degradation rates to avoid bed defluidization [57, 58]. This result is explained by the

357 more branched structure of PP compared to polyethylene, which makes it a more

358 degradable polyolefin [59-61]. In fact, cracking takes place firstly in the branched chain

359 followed by the main chain. Another explanation of the lower degradation temperature

360 lies in the higher proportion of tertiary carbons in the polypropylene chains, which

361 promote the thermal cleavage of C–C bonds [62]. Similarly, LDPE undergoes a slightly

362 higher degradation rate than HDPE due to the reactivity caused by branching and

363 tertiary carbons in its structure [62].

364 PET degradation occurred between 385 and 520 ºC (Figure 5), and the pyrolysis

365 temperature in the CSBR needed to be at least 710 ºC under the *base case* conditions in

366 order to avoid bed collapse (Figure 5). Unlike other polymers, the pyrolysis of PET in

367 the CSBR led to the formation of a stable solid residue of sticky nature, which can

368 easily form aggregates with sand [63]. As the pyrolysis progressed, and simultaneously

369 to polymer cracking, aggregates composed of a sticky carbon residue and sand particles

370 were formed, which joined together to form bigger aggregates and caused difficulties in

371 the spouting, firstly by clogging the draft tube and then collapsing the bed [10].

372 Increasing the reaction temperature accelerated polymer degradation and reduced the

373 formation of the solid residue. Thus, temperatures above 710 ºC lowered the yield of

374 this residue and avoided its capacity to form bigger aggregates leading to bed

375 defluidization [20]. In fact, under these conditions, the pyrolysis reaction is much faster

376 than the PET repolymerization that causes the formation of stable carbon material and

377 covers the sand particles. Consequently, pyrolysis is more efficient at high temperatures

378 and the result is a reduction in the solid residue. Once PET pyrolysis has been

379 completed, the solid residue is burnt in the CSBR reactor itself by feeding an air stream.

380 The degradation sequence that a polymer undergoes in gas-solid reactors, such as FBR

381 or CSBR, differs depending on the polymer type and is conditioned by the interactions

382 between the plastic and the inert or catalyst particles in the bed. Indeed, the physical

383 properties (viscosity and thermal conductivity) during thermal degradation depend on

384 the type of polymer, and they play a key role in the defluidization sequence. Heat

385 transfer restrictions and agglomerate formation depend on the mentioned properties, and

386 they therefore depend on the type of plastic. According to Arena and Mallestone [20,

23, 26, 64], defluidization follows different mechanisms depending on the polymer type, and the degradation rate depends on the operating conditions. In the case of polyolefins, they do not produce a sticky solid residue and the initial aggregates undergo fast crumbling into smaller sizes depending on the operating conditions (temperature, heating rate, $W_{bed}/Q_{plastic}$, etc.), and the sintering of sand particles covered by a layer of adhesive residue may occur, worsening the fluidization quality until defluidization. Nevertheless, these authors did not observe crumbling during PET pyrolysis, as the sticky solid residue was adhered to the sand particles and led to the formation of polymer-sand aggregates at rather low reaction temperatures (between 450 and 650 ℃), which rapidly grow to form bigger ones. When a critical fraction of the bed are large agglomerates, the bed defluidizes. These authors also concluded that an increase in temperature changed progressively the defluidization mechanism of PET polymer. Thus, at low temperatures the aggregates played the main role in defluidization, but the accumulation of large aggregates decreased as temperature was increased and the worsening of fluidization was mainly due to the progressive increase in the polymeric layer on the sand, as was the case for polyolefins.

The results of this study highlight that the formation of plastic-sand aggregates for polyolefins and PET in a fountain confined CSBR is similar to that observed in fluidized beds. Besides, the degradation steps for PMMA and PS were analogous to those for polyolefins, as the sticky solid residue was not generated under the *base case* operating conditions. The degradation rate of the polymers at the operating temperatures shown in Figure 6 was high enough to avoid the formation of large aggregates leading to bed defluidization. However, the defluidization mechanism in the CSBR technology is different depending on whether a draft tube is used or not. When no draft tube is used, the defluidization mechanism is the same as that observed by Arena and Mastellone [20,

412 23, 26, 64], i.e., the formation of polymer-sand aggregates and their growth, with their

413 spouting velocity being much higher than that for the individual particle beds. These

414 aggregates are too large to spout and lead to bed collapse. Nevertheless, when the draft

415 tube was used for plastic pyrolysis, defluidization occurred by tube clogging, and the

416 subsequent formation of a plug on the upper surface of the bed. From that moment, any

417 plastic fed into the reactor accumulated on the bed surface.

418 The operating temperatures for stable operation without particle agglomeration are

419 slightly higher compared to those in conventional spouted beds (between 10 and 20 ºC

420 higher) [54, 55]. Therefore, higher temperatures are required to increase the degradation

421 rate of polymers and avoid the formation of large aggregates. However, the insertion of

422 a fountain confiner and a non-porous draft tube allowed operating with finer sand

423 particles, and therefore lower nitrogen flow rates. Thus, we used a sand particle size of

424 0.2-0.3 mm or even lower, with a nitrogen flow rate of 10 L min^{-1} (u/u_{ms} = 4), whereas

425 conventional CSBRs require sand particles bigger than 0.6 mm and nitrogen flow rates

426 ranging from 12 to 24 L min^{-1} (u/u_{ms} from 1.2 to 2). Likewise, fluidized bed reactors

427 also require higher temperatures and/or higher nitrogen flow rates to avoid bed

428 defluidization in the pyrolysis of the same plastics used in this study [18, 20, 26, 53, 65,

429 66].

430 **3.2. Effect of $W_{bed}/Q_{plastic}$ ratio**

431 Runs were conducted using HDPE feed rates ($Q_{plastic}$) ranging from 0.5 g min^{-1} to 3 g

432 min^{-1} and sand beds of 100 and 250 g with a particle size in the 0.2-0.3 mm range. As

433 shown in Table 3, the nitrogen flow rate ranged from 8 to 11.2 L min^{-1} in order to

434 maintain a u/u_{ms} ratio of 4 with the two bed masses.

Figure 7 shows the minimum temperature for stable operation to avoid defluidization for different $W_{bed}/Q_{plastic}$ ratios. As observed, an increase in this parameter (either by reducing the plastic feed rate or by increasing the bed mass) reduced the pyrolysis temperature required to ensure a good bed performance. Indeed, for a $W_{bed}/Q_{plastic}$ ratio of 50 min (HDPE feed rate of 3 g min^{-1} and 150 g of inert sand), the temperature needed was 570 ℃, but for a ratio of 300 min (HDPE feed rate of 0.5 g min^{-1} and 150 g of inert sand), the temperature was reduced by 70 ℃ for operating under the same hydrodynamic state (4 times the minimum spouting velocity). Similarly, when the bed mass was increased from 100 g ($W_{bed}/Q_{plastic}$=100 min) to 250 g ($W_{bed}/Q_{plastic}$=250 min), the minimum temperature for stable operation was reduced from 530 to 510 ℃.
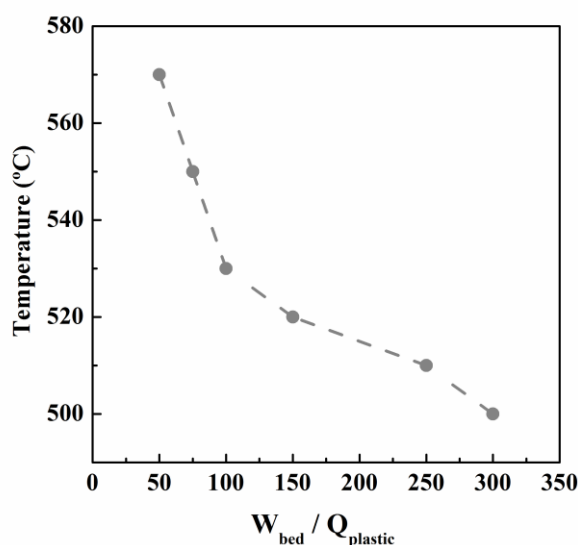
Figure 7. Minimum temperature for stable operation in the fast pyrolysis of HDPE with different ratios of bed mass to plastic feed rate.

According to Arena et al. [26], high plastic feed rates lead to thick layers of polymer deposited on the surface of bed particles. The critical thickness is the value above which the particles fuse when they collide, and is a function of plastic viscosity and the momentum of the colliding particles. If the thickness of the viscous layer coating the

452   sand is greater than the critical one corresponding to the operating conditions, the

453   relative velocity of the particles is too low to overcome the viscous adhesion of the

454   bridge between the surfaces and they stick to each other, thus accelerating the formation

455   of bigger aggregates. Nevertheless, a bed with a high amount of sand promotes solid

456   circulation, especially in the fountain region, thus enhancing the turbulence and fluid-

457   particle interaction, which leads to a higher degradation rate of the viscous polymer and

458   avoids the formation of bigger aggregates. In fact, polymer heating is improved, which

459   enhances the effective reaction rate of plastic degradation, thus lowering the

460   temperature required to complete pyrolysis. Hence, when the $W_{bed}/Q_{plastic}$ ratio is

461   reduced, the operating temperature must be raised to increase polymer degradation rate

462   and provide more energy, which helps to reduce the viscosity of the fused polymer.

463   Comparing the results of HDPE pyrolysis in the fountain confined and conventional

464   CSBRs, the former requires higher $W_{bed}/Q_{plastic}$ ratios for operating at the same

465   temperature [67, 68]. However, the sand particle size and, especially, the nitrogen flow

466   rate required are much higher in the conventional spouted bed under the same

467   hydrodynamic conditions (u/u_{ms}).

468   **3.3. Effect of spouting velocity**

469   The gas flow rate used in the pyrolysis is an essential parameter for a suitable spouting

470   behavior. Runs were carried out using flow rates in the range from 1.2 to 4 times the

471   minimum velocity, with the other operating parameters being fixed at the value of the

472   *base case*. The nitrogen flow rates used are shown in Table 3. Note that nitrogen is used

473   at laboratory scale, but recirculation of the pyrolysis gases for use as fluidizing agent is

474   a more feasible strategy on a larger scale pyrolysis process, thus minimizing nitrogen

475   requirements. This strategy was successfully applied in a 25 kg/h biomass fast pyrolysis

476 CSBR pilot plant, in which part of the non-condensable gases where recirculated and

477 the excess gas was purged and burnt in a flare [69].

478 Figure 8 shows the minimum temperature for stable operation at different u/u_{ms} ratios.

479 As observed, the temperature to ensure a good bed performance was 550 ºC for a

480 velocity 1.2 higher than the minimum one, but decreased to 530 ºC and 520 ºC when the

481 u/u_{ms} ratio was increased to 1.6 and 2, respectively. No improvement was observed for

482 higher gas velocities, with the minimum operating temperature being 520 ºC. This

483 performance is explained by the low turbulence and solid circulation rate at gas

484 velocities close to the minimum one. In this case, particles motion is smoother and they

485 describe shorter trajectories in the fountain, thereby requiring higher temperatures to

486 increase both the degradation rate of the polymer and the critical thickness of the plastic

487 layer on the particle in order to avoid the formation of aggregates. Once a vigorous

488 spouting regime was attained with a u/u_{ms} ratio of 2, the vigorous movement of the

489 solid, especially in the fountain region, was enough to break the aggregates made up of

490 sand and melted plastic, thus allowing a stable operation at lower temperatures.

491 Furthermore, these conditions allowed a uniform distribution of the fused plastic in the

492 bed, thus favoring the initial physical steps in the pyrolysis process. ~~Nevertheless, an~~

493 ~~increase in gas velocity in fluidized beds does not lead to significant improvement in the~~

494 ~~fluidization quality of the aggregates, as most of the excess gas rises through the bed in~~

495 ~~the bubble phase and particle velocity hardly changes [20].~~

496
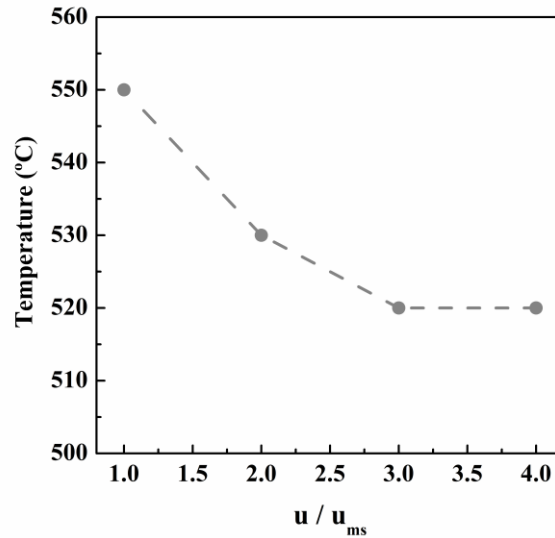
Figure 8. Minimum temperature for stable operation at different u/u_{ms} ratios.

498 An increase in gas velocity leads to a more vigorous solid circulation, which improves

499 heat transfer in the bed. In fact, as the heating rate of plastic particles is higher, the time

500 required for plastic degradation is shorter, thus minimizing its accumulation in the bed

501 and attenuating the growth of aggregates leading to defluidization. Saldarriaga et al.

502 [70] observed an increase in heat transfer coefficient as gas velocity is increased in

503 conical spouted beds of sawdust+sand. According to these authors, the average values

504 of bed-to-surface heat transfer coefficient are 203 W/m^2 K for sawdust and 505 W/m^2 K

505 for sand, which are high enough values for attaining high heating rates in

506 thermochemical processes. Moreover, the high velocity of the particles when turbulence

507 is increased generates more collisions and enhances the effective reaction rate of plastic

508 pyrolysis. This issue together with the faster heating rate of the particles leads to an

509 increase in the critical thickness of the plastic layer, thus reducing agglomeration

510 problems. Nevertheless, an increase in gas velocity in fluidized beds does not lead to

511 significant improvement in the fluidization quality of the aggregates, as most of the

512 excess gas rises through the bed in the bubble phase and particle velocity hardly

513 changes [20].

3.4. Effect of catalyst loading

515 The interest in using a fountain confiner for plastics pyrolysis in spouted beds is related

516 to the improvement in catalyst efficiency. Accordingly, the influence of the catalyst on

517 bed defluidization was also analyzed. Thus, different amounts of spent FCC catalyst (0,

518 7, 15 and 30 g) with a particle size in the 90 - 150 μm range were loaded into the bed.

519 The total bed mass in all runs was 150 g, which was made up of sand with a particle

520 size in the 0.2 - 0.3 mm range and the mentioned amount of catalyst. The other

521 operating parameters were the same as in the *base case* (1 g min^{-1} of HDPE and a u/u$_{ms}$

522 of 4). The gas flow rate to attain a u/u$_{ms}$ of 4 is considerable lower than in the base case

523 (7 L min^{-1} instead of 10 L min^{-1}) due to the lower particle size and density of the FCC

524 catalyst. It is noteworthy that draft tubes ease the handling of solids with different sizes

525 and densities without stability problems [71].

526 Figure 9 shows the influence the amount of spent FCC catalyst (space time) has on the

527 minimum temperature for stable operation in the pyrolysis of HDPE. As observed, the

528 minimum temperature decreases linearly for small and moderate amounts of catalyst

529 (from 520 ºC without catalyst to 480 ºC when 15 g of catalyst were loaded). The

530 decreasing trend is smoother for higher amounts (460 ºC when the space time is 30 min

531 g$_{cat}$ g$_{plastic}$$^{-1}$). The moderate acidity of the spent FCC catalyst makes catalytic cracking to

532 occur through a carbocationic mechanism (mainly by carbenium ions) instead of the

533 free radical mechanism characteristic to the thermal cracking in pyrolysis processes

534 [72]. Hence, catalytic cracking takes place with a lower activation energy than thermal

535 cracking, and so at lower temperatures. Therefore, catalysts *in situ* accelerate fused

536 polymer conversion to volatile products and avoid its accumulation in the bed.

537 Furthermore, the vigorous solid circulation in the spouted bed reactor also contributes to

538 improving the contact between the melted plastic and the catalyst, and therefore to

539 enhancing the cracking of fused polymer chains to volatile products.
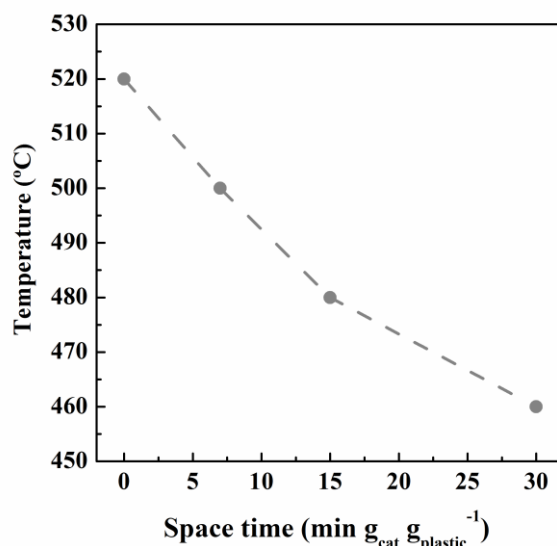
540

541 **Figure 9**. Evolution of the temperature for stable operation with the mass of spent FCC

542 catalyst loaded in the bed.

543 The significant reduction in the minimum temperature for stable operation caused by the

544 FCC catalyst is consistent with the results obtained in TGA runs. As observed in Figure

545 10, the incorporation of 5 mg of FCC to the polymer sample markedly reduced the

546 pyrolysis temperature compared to the catalyst free one. Indeed, the degradation of the

547 sample with catalyst started at 400 °C and the maximum degradation rate was attained at

548 458 °C, whereas for the catalyst free sample these temperatures were 420 °C and 493 °C,

549 respectively. Thus, it can be concluded that the catalyst influences both the primary

550 polymer degradation and the secondary conversion of pyrolysis volatiles towards

551 valuable products. The primary activity of the catalytic is evidenced by the acceleration

552 of polymer degradation observed in the TGA analysis (Figure 10), whose

28

553 devolatilization took place at lower temperatures in contact with the catalysts. In the

554 same line, the catalysts presence in the experiments performed in the CSBR allowed for

555 operating at lower temperatures, which is associated with the polymer degradation

556 favored by the catalyst (Figure 9). These results clearly show the capacity of the catalyst

557 to promote plastic decomposition even under the severe mass transfer limitations

558 associated with the fused polymer-catalyst contact.
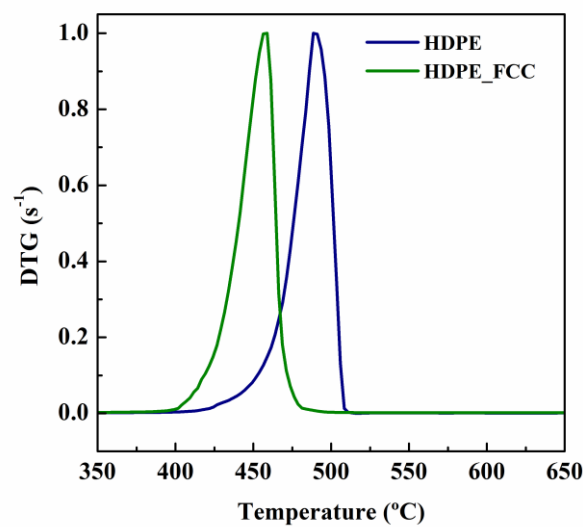
559

560 **Figure 10**. DTG curves for HDPE degradation loaded with 5 mg of FCC catalyst and

561 without catalyst loading.

562 **3.5. Fountain confined CSBR for plastic pyrolysis**

563 The insertion of a fountain confiner and non-porous draft tube in the CSBR allows

564 increasing the turbulence in the bed, thus increasing the solid circulation, which

565 promotes the contact between the sand (or catalyst) and the melted plastic, as well as the

566 heat transfer rate [73, 74]. Moreover, the fountain confiner allows operating with much

567 finer catalyst particles than in conventional conical spouted beds without entrainment

568 problems. This positive effect of particle size reduction for improving heat transfer, gas-

569   solid contact, and therefore feedstock conversion, has already been described in

570   fluidized beds used in biomass and coal gasification processes [75, 76]. Therefore,

571   operation with smaller catalyst particles promotes the contact between the melted

572   polymer and the catalyst, and lower spouting gas flow rates than in conventional CSBRs

573   are required. Thus, Elordi et al [77] performed satisfactorily the catalytic cracking of

574   polyethylene on a spent FCC catalyst in a conventional CSBR, but they had to

575   agglomerate the original FCC catalyst particles to the 0.6−1.2 mm size by wet

576   extrusion. In the present study, the particle size of the catalyst was as collected in the

577   purge at the exit of the FCC unit regenerator, where most of the particles (93 wt %) are

578   in the 20−149 μm range, with an average diameter of 81 μm. Moreover, another

579   advantage of confining the fountain is that the gas is forced to flow down to leave the

580   confiner through its bottom, which increases the volatile residence time in contact with

581   the catalyst. This point is of great significance, since it promotes cracking reactions

582   [33]. Besides, the vigorous movement of the solids at the fountain enhanced regime

583   improves the gas-solid contact and leads to faster and homogeneous coating of the

584   particles with the melted plastic, thus increasing the efficiency of the catalyst.

585   Therefore, the fountain confined spouted bed is an interesting and novel reactor design

586   for the catalytic valorizations of waste plastics due its capacity to overcome

587   defluidization problems.

588   Moreover, although defluidization in the thermal pyrolysis occurred faster with the

589   fountain confined system than with conventional CSBR, as the aggregates blocked the

590   draft tube and required slightly higher temperatures to avoid this problem, the reduction

591   of nitrogen flow rate, as well as the smaller bed particle sizes used without fine

592   entrainment, are interesting advantages of this system. However, the great advantage of

593   this work lies in the good performance of fountain confined CSBR in the catalytic

594 pyrolysis of waste plastics. Particularly, this work evidences that, under pyrolysis

595 conditions, the fountain confined system allows working with catalyst at low

596 temperatures without defluidization problems due to the adequate contact between

597 plastic and catalyst particles, which enhances the efficiency of the catalyst and promotes

598 the cracking of fused polymer chains to volatile products.

599 **5. Conclusions**

600 Conventional CSBRs have been proven to perform well in the pyrolysis of waste

601 plastics due to their high heat-transfer rates and bed turbulence, which avoids particle

602 agglomeration and segregation problems. However, the insertion of a fountain confiner

603 in the CSBR for plastic pyrolysis allowed: i) operating with finer materials (sand and

604 catalyst); ii) increasing the u/u_{ms} ratio to 4 without elutriation; iii) improving bed

605 turbulence and gas-solid contact, especially in the fountain region; and iv) providing

606 great stability to the bed. Accordingly, the optimum hydrodynamic conditions for stable

607 operation in order to avoid particle agglomeration and bed defluidization were

608 established in a fountain confined CSBR. The minimum temperature for stable

609 operation was delimited depending on the plastic type, feed rate, bed mass, spouting

610 velocity and presence of catalyst.

611 PMMA and PS required the lowest temperatures to avoid bed defluidization, followed

612 by polyolefins, for which the operating temperature ranged from 500 to 520 ºC. In the

613 pyrolysis of PET, a higher temperature was required to minimize the formation of a

614 stable solid residue of sticky nature, which easily forms aggregates with the sand, thus

615 worsening bed performance. Regarding the $W_{bed}/Q_{plastic}$ ratio, an increase in this

616 parameter reduces the temperature required to ensure a good bed performance, as the

617 thickness of the viscous layer that coats the sand is reduced, thereby hindering the

formation of bigger aggregates. Moreover, an increase in gas velocity increased the turbulence in the bed and the particles were able to describe longer trajectories, improving the gas-solid contact and lowering the temperature required to avoid bed defluidization. The use of a spent FCC catalyst promoted cracking reactions that require lower activation energies, and therefore the pyrolysis takes place at lower temperatures. The superior contact with the catalysts reached in the fountain confined spouted bed allowed for a remarkable reduction in pyrolysis temperature. Although the novel confinement system has certain limitations for thermal pyrolysis, its performance is outstanding in the catalytic pyrolysis of waste plastics. Thus, the fountain enhanced regime, in which a significant fraction of the bed is in the fountain, greatly promotes the cracking of fused polymer chains.

636   **References**

637   [1] C.J. Moore, Synthetic polymers in the marine environment: A rapidly increasing, long-term
638   threat, Environ. Res. 108 (2008) 131-139.

639   [2] R. Miandad, M.A. Barakat, A.S. Aburiazaiza, M. Rehan, A.S. Nizami, Catalytic pyrolysis of
640   plastic waste: A review, Process Saf. Environ. Prot. 102 (2016) 822-838.

641   [3] G. Lopez, M. Artetxe, M. Amutio, J. Alvarez, J. Bilbao, M. Olazar, Recent advances in the
642   gasification of waste plastics. A critical overview, Renewable Sustainable Energy Rev 82
643   (2018) 576-596.

644   [4] R. Verma, K.S. Vinoda, M. Papireddy, A.N.S. Gowda, Toxic Pollutants from Plastic Waste-
645   A Review, Procedia Environ. Sci. 35 (2016) 701-708.

646   [5] I. Barbarias, G. Lopez, M. Artetxe, A. Arregi, J. Bilbao, M. Olazar, Valorisation of different
647   waste plastics by pyrolysis and in-line catalytic steam reforming for hydrogen production,
648   Energy Convers. Manage. 156 (2018) 575-584.

649   [6] S.M. Al-Salem, A. Antelava, A. Constantinou, G. Manos, A. Dutta, A review on thermal
650   and catalytic pyrolysis of plastic solid waste (PSW), J. Environ. Manage. 197 (2017) 177-198.

651   [7] M. Al-asadi, N. Miskolczi, Z. Eller, Pyrolysis-gasification of wastes plastics for syngas
652   production using metal modified zeolite catalysts under different ratio of nitrogen/oxygen, J.
653   Clean. Prod. 271 (2020).

654   [8] S. Kumagai, R. Yamasaki, T. Kameda, Y. Saito, A. Watanabe, C. Watanabe, N. Teramae, T.
655   Yoshioka, Catalytic Pyrolysis of Poly(ethylene terephthalate) in the Presence of Metal Oxides
656   for Aromatic Hydrocarbon Recovery Using Tandem μ-Reactor-GC/MS, Energy Fuels 34 (2020)
657   2492-2500.

658   [9] S. Jung, M. Cho, B. Kang, J. Kim, Pyrolysis of a fraction of waste polypropylene and
659   polyethylene for the recovery of BTX aromatics using a fluidized bed reactor, Fuel Process.
660   Technol. 91 (2010) 277-284.

661   [10] M. Artetxe, G. Lopez, M. Amutio, G. Elordi, M. Olazar, J. Bilbao, Operating conditions for
662   the pyrolysis of poly-(ethylene terephthalate) in a conical spouted-bed reactor, Ind. Eng. Chem.
663   Res. 49 (2010) 2064-2069.

664   [11] J.M. Saad, M.A. Nahil, P.T. Williams, Influence of process conditions on syngas
665   production from the thermal processing of waste high density polyethylene, J. Anal. Appl.
666   Pyrolysis 113 (2015) 35-40.

667   [12] Y. Zhang, G. Ji, C. Chen, Y. Wang, W. Wang, A. Li, Liquid oils produced from pyrolysis
668   of plastic wastes with heat carrier in rotary kiln, Fuel Process. Technol. 206 (2020) 106455.

669   [13] Y. Zhang, G. Ji, D. Ma, C. Chen, Y. Wang, W. Wang, A. Li, Exergy and energy analysis of
670   pyrolysis of plastic wastes in rotary kiln with heat carrier, Process Saf. Environ. Prot. 142
671   (2020) 203-211.

672   [14] D.P. Serrano, J. Aguado, J.M. Escola, E. Garagorri, Conversion of low density
673   polyethylene into petrochemical feedstocks using a continuous screw kiln reactor, J. Anal. Appl.
674   Pyrolysis 58-59 (2001) 789-801.

675   [15] A. Undri, L. Rosi, M. Frediani, P. Frediani, Efficient disposal of waste polyolefins through
676   microwave assisted pyrolysis, Fuel 116 (2014) 662-671.

677   [16] G. Lopez, M. Artetxe, M. Amutio, J. Bilbao, M. Olazar, Thermochemical routes for the
678   valorization of waste polyolefinic plastics to produce fuels and chemicals. A review, Renewable
679   Sustainable Energy Rev 73 (2017) 346-368.

680   [17] M.S. Qureshi, A. Oasmaa, H. Pihkola, I. Deviatkin, A. Tenhunen, J. Mannila, H.
681   Minkkinen, M. Pohjakallio, J. Laine-Ylijoki, Pyrolysis of plastic waste: Opportunities and
682   challenges, J. Anal. Appl. Pyrolysis (2020) 104804.

683   [18] T. Yoshioka, G. Grause, C. Eger, W. Kaminsky, A. Okuwaki, Pyrolysis of poly(ethylene
684   terephthalate) in a fluidised bed plant, Polym. Degrad. Stab. 86 (2004) 499-504.

685   [19] W. Kaminsky, Chemical recycling of mixed plastics of pyrolysis, Adv. Polym. Technol. 14
686   (1995) 337-344.

687   [20] U. Arena, M.L. Mastellone, Defluidization phenomena during the pyrolysis of two plastic
688   wastes, Chem. Eng. Sci. 55 (2000) 2849-2860.

689   [21] M. Bartels, W. Lin, J. Nijenhuis, F. Kapteijn, J.R. van Ommen, Agglomeration in fluidized
690   beds at high temperatures: Mechanisms, detection and prevention, Prog. Energy Combust. Sci.
691   34 (2008) 633-666.

692   [22] U. Arena, A. Cammarota, M.L. Mastellone, The phenomenology of comminution in the
693   fluidized bed combustion of packaging-derived fuels, Fuel 77 (1998) 1185-1193.

694   [23] M.L. Mastellone, U. Arena, Bed defluidisation during the fluidised bed pyrolysis of plastic
695   waste mixtures, Polym. Degradation Stab. 85 (2004) 1051-1058.

696   [24] S. Weber, C. Briens, F. Berruti, E. Chan, M. Gray, Agglomerate stability in fluidized beds
697   of glass beads and silica sand, Powder Technol. 165 (2006) 115-127.

698   [25] J.P.K. Seville, C.D. Willett, P.C. Knight, Interparticle forces in fluidisation: a review,
699   Powder Technol. 113 (2000) 261-268.

700   [26] U. Arena, M.L. Mastellone, The phenomenology of bed defluidization during the pyrolysis
701   of a food-packaging plastic waste, Powder Technol. 120 (2001) 127-133.

702   [27] R. Aguado, R. Prieto, M.J.S. José, S. Alvarez, M. Olazar, J. Bilbao, Defluidization
703   modelling of pyrolysis of plastics in a conical spouted bed reactor, Chem. Eng. Process. 44
704   (2005) 231-235.

705   [28] M. Olazar, Measurement of particle velocities in conical spouted beds using an optical fiber
706   probe, Ind. Eng. Chem. Res. 37 (1998) 4520-4527.

707   [29] H. Altzibar, I. Estiati, G. Lopez, J.F. Saldarriaga, R. Aguado, J. Bilbao, M. Olazar,
708   Fountain confined conical spouted beds, Powder Technol. 312 (2017) 334-346.

709   [30] H. Altzibar, G. Lopez, R. Aguado, S. Alvarez, M.J. San Jose, M. Olazar, Hydrodynamics
710   of conical spouted beds using different types of internal devices, Chem. Eng. Technol. 32
711   (2009) 463-469.

712   [31] H. Altzibar, G. Lopez, J. Bilbao, M. Olazar, Minimum spouting velocity of conical spouted
713   beds equipped with draft tubes of different configuration, Ind. Eng. Chem. Res. 52 (2013) 2995-
714   3006.

715   [32] H. Altzibar, G. Lopez, J. Bilbao, M. Olazar, Operating and peak pressure drops in conical
716   spouted beds equipped with draft tubes of different configuration, Ind. Eng. Chem. Res 53
717   (2014) 415-427.

718   [33] M. Cortazar, G. Lopez, J. Alvarez, M. Amutio, J. Bilbao, M. Olazar, Advantages of
719   confining the fountain in a conical spouted bed reactor for biomass steam gasification, Energy
720   (2018).

721   [34] M. Tellabide, I. Estiati, A. Pablos, H. Altzibar, R. Aguado, M. Olazar, New operation
722   regimes in fountain confined conical spouted beds, Chem. Eng. Sci. 211 (2020) 115255.

723   [35] K. Azizi, M. Keshavarz Moraveji, A. Arregi, M. Amutio, G. Lopez, M. Olazar, On the
724   pyrolysis of different microalgae species in a conical spouted bed reactor: bio-fuel yields and
725   characterization, Bioresour. Technol. (2020) 123561.

726   [36] G. Lopez, M. Cortazar, J. Alvarez, M. Amutio, J. Bilbao, M. Olazar, Assessment of a
727   conical spouted with an enhanced fountain bed for biomass gasification, Fuel 203 (2017) 825-
728   831.

729   [37] M. Cortazar, G. Lopez, J. Alvarez, M. Amutio, J. Bilbao, M. Olazar, Behaviour of primary
730   catalysts in the biomass steam gasification in a fountain confined spouted bed, Fuel 253 (2019)
731   1446-1456.

732   [38] M. Cortazar, J. Alvarez, G. Lopez, M. Amutio, L. Santamaria, J. Bilbao, M. Olazar, Role
733   of temperature on gasification performance and tar composition in a fountain enhanced conical
734   spouted bed reactor, Energy Convers. Manage. 171 (2018) 1589-1597.

735   [39] J. Alvarez, M. Amutio, G. Lopez, J. Bilbao, M. Olazar, Fast co-pyrolysis of sewage sludge
736   and lignocellulosic biomass in a conical spouted bed reactor, Fuel 159 (2015) 810-818.

737   [40] J. Alvarez, G. Lopez, M. Amutio, N.M. Mkhize, B. Danon, P. van der Gryp, J.F. Görgens,
738   J. Bilbao, M. Olazar, Evaluation of the properties of tyre pyrolysis oils obtained in a conical
739   spouted bed reactor, Energy 128 (2017) 463-474.

740   [41] J. Alvarez, G. Lopez, M. Amutio, J. Bilbao, M. Olazar, Bio-oil production from rice husk
741   fast pyrolysis in a conical spouted bed reactor, Fuel 128 (2014) 162-169.

742   [42] G. Elordi, M. Olazar, G. Lopez, M. Artetxe, J. Bilbao, Continuous polyolefin cracking on
743   an HZSM-5 zeolite catalyst in a conical spouted bed reactor, Ind. Eng. Chem. Res. 50 (2011)
744   6061-6070.

745   [43] M. Amutio, G. Lopez, J. Alvarez, R. Moreira, G. Duarte, J. Nunes, M. Olazar, J. Bilbao,
746   Flash pyrolysis of forestry residues from the Portuguese Central Inland Region within the
747   framework of the BioREFINA-Ter project, Bioresour. Technol. 129 (2013) 512-518.

748   [44] G. Lopez, J. Alvarez, M. Amutio, N.M. Mkhize, B. Danon, P. van der Gryp, J.F. Görgens,
749   J. Bilbao, M. Olazar, Waste truck-tyre processing by flash pyrolysis in a conical spouted bed
750   reactor, Energy Convers. Manage. 142 (2017) 523-532.

751 [45] H. Altzibar, I. Estiati, G. Lopez, J.F. Saldarriaga, R. Aguado, J. Bilbao, M. Olazar,
752 Fountain confined conical spouted beds, Powder Technol. 312 (2017) 334-346.

753 [46] J. Shabanian, P. Sauriol, A. Rakib, J. Chaouki, Application of temperature and pressure
754 signals for early detection of defluidization conditions, Procedia Eng. 102 (2015) 1006-1015.

755 [47] G. Elordi, M. Olazar, P. Castaño, M. Artetxe, J. Bilbao, Polyethylene cracking on a spent
756 FCC catalyst in a conical spouted bed, Ind. Eng. Chem. Res. 51 (2012) 14008-14017.

757 [48] R. Chirone, F. Miccio, F. Scala, Mechanism and prediction of bed agglomeration during
758 fluidized bed combustion of a biomass fuel: Effect of the reactor scale, Chem. Eng. J. 123
759 (2006) 71-80.

760 [49] J. Shabanian, P. Sauriol, J. Chaouki, A simple and robust approach for early detection of
761 defluidization, Chem. Eng. J. 313 (2017) 144-156.

762 [50] G. Tardos, D. Mazzone, R. Pfeffer, Destabilization of fluidized beds due to agglomeration
763 part II: Experimental verification, Can. J. Chem. Eng. 63 (1985) 384-389.

764 [51] J.H. Siegell, High-temperature de fluidization, Powder Technol. 38 (1984) 13-22.

765 [52] P. Kasar, D.K. Sharma, M. Ahmaruzzaman, Thermal and catalytic decomposition of waste
766 plastics and its co-processing with petroleum residue through pyrolysis process, J. Clean. Prod.
767 265 (2020) 121639.

768 [53] B. Kang, S.G. Kim, J. Kim, Thermal degradation of poly(methyl methacrylate) polymers:
769 Kinetics and recovery of monomers using a fluidized bed reactor, J. Anal. Appl. Pyrolysis 81
770 (2008) 7-13.

771 [54] G. Lopez, M. Artetxe, M. Amutio, G. Elordi, R. Aguado, M. Olazar, J. Bilbao, Recycling
772 poly-(methyl methacrylate) by pyrolysis in a conical spouted bed reactor, Chem. Eng. Process. :
773 Process Intensif. 49 (2010) 1089-1094.

774 [55] M. Artetxe, G. Lopez, M. Amutio, I. Barbarias, A. Arregi, R. Aguado, J. Bilbao, M.
775 Olazar, Styrene recovery from polystyrene by flash pyrolysis in a conical spouted bed reactor,
776 Waste Manag. 45 (2015) 126-133.

777 [56] M. Marczewski, E. Kamińska, H. Marczewska, M. Godek, G. Rokicki, J. Sokołowski,
778 Catalytic decomposition of polystyrene. The role of acid and basic active centers, Appl. Catal. B
779 129 (2013) 236-246.

780 [57] A. Aboulkas, K. El harfi, A. El Bouadili, Thermal degradation behaviors of polyethylene
781 and polypropylene. Part I: Pyrolysis kinetics and mechanisms, Energy Convers. Manage. 51
782 (2010) 1363-1369.

783 [58] F. Xu, B. Wang, D. Yang, J. Hao, Y. Qiao, Y. Tian, Thermal degradation of typical plastics
784 under high heating rate conditions by TG-FTIR: Pyrolysis behaviors and kinetic analysis,
785 Energy Convers. Manage. 171 (2018) 1106-1115.

786 [59] I. Hakki Metecan, A.R. Ozkan, R. Isler, J. Yanik, M. Saglam, M. Yuksel, Naphtha derived
787 from polyolefins, Fuel 84 (2005) 619-628.

788   [60] I. Ahmad, M.I. Khan, H. Khan, M. Ishaq, R. Tariq, K. Gul, W. Ahmad, Pyrolysis Study of
789   Polypropylene and Polyethylene Into Premium Oil Products, Int. J. Green Energy 12 (2015)
790   663-671.

791   [61] M. Arabiourrutia, G. Elordi, G. Lopez, E. Borsella, J. Bilbao, M. Olazar, Characterization
792   of the waxes obtained by the pyrolysis of polyolefin plastics in a conical spouted bed reactor, J.
793   Anal. Appl. Pyrolysis 94 (2012) 230-237.

794   [62] J. Aguado, D.P. Serrano, J.M. Escola, E. Garagorri, J.A. Fernández, Catalytic conversion
795   of polyolefins into fuels over zeolite beta, Polym. Degrad. Stab. 69 (2000) 11-16.

796   [63] P.T. Williams, E.A. Williams, Interaction of plastics in mixed-plastics pyrolysis, Energy
797   Fuels 13 (1999) 188-196.

798   [64] M.L. Mastellone, U. Arena, Fluidized-bed pyrolysis of polyolefins wastes: Predictive
799   defluidization model, AIChE J. 48 (2002) 1439-1447.

800   [65] W. Kaminsky, M. Predel, A. Sadiki, Feedstock recycling of polymers by pyrolysis in a
801   fluidised bed, Polym. Degrad. Stab. 85 (2004) 1045-1050.

802   [66] F.J. Mastral, E. Esperanza, P. García, M. Juste, Pyrolysis of high-density polyethylene in a
803   fluidised bed reactor. Influence of the temperature and residence time, J. Anal. Appl. Pyrolysis
804   63 (2002) 1-15.

805   [67] M. Artetxe, G. Lopez, G. Elordi, M. Amutio, J. Bilbao, M. Olazar, Production of light
806   olefins from polyethylene in a two-step process: Pyrolysis in a conical spouted bed and
807   downstream high-temperature thermal cracking, Ind. Eng. Chem. Res. 51 (2012) 13915-13923.

808   [68] G. Elordi, M. Olazar, G. Lopez, M. Artetxe, J. Bilbao, Product yields and compositions in
809   the continuous pyrolysis of high-density polyethylene in a conical spouted bed reactor, Ind.
810   Eng. Chem. Res. 50 (2011) 6650-6659.

811   [69] A.R. Fernandez-Akarregi, J. Makibar, G. Lopez, M. Amutio, M. Olazar, Design and
812   operation of a conical spouted bed reactor pilot plant (25 kg/h) for biomass fast pyrolysis, Fuel
813   Process Technol 112 (2013) 48-56.

814   [70] J.F. Saldarriaga, J. Grace, C.J. Lim, Z. Wang, N. Xu, A. Atxutegi, R. Aguado, M. Olazar,
815   Bed-to-surface heat transfer in conical spouted beds of biomass–sand mixtures, Powder
816   Technol. 283 (2015) 447-454.

817   [71] A. Atxutegi, M. Tellabide, G. Lopez, R. Aguado, J. Bilbao, M. Olazar, Implementation of a
818   borescopic technique in a conical spouted bed for tracking spherical and irregular particles,
819   Chem. Eng. J. 374 (2019) 39-48.

820   [72] T. Ueno, E. Nakashima, K. Takeda, Quantitative analysis of random scission and chain-end
821   scission in the thermal degradation of polyethylene, Polym. Degrad. Stab. 95 (2010) 1862-1869.

822   [73] T. Ishikura, H. Nagashima, M. Ide, Hydrodynamics of a spouted bed with a porous draft
823   tube containing a small amount of finer particles, Powder Technol. 131 (2003) 56-65.

824   [74] C.A. Da Rosa, J.T. Freire, Fluid dynamics analysis of a draft-tube continuous spouted bed
825   with particles bottom feed using CFD, Ind. Eng. Chem. Res. 48 (2009) 7813-7820.

826 [75] S. Koppatz, J.C. Schmid, C. Pfeifer, H. Hofbauer, The effect of bed particle inventories
827 with different particle sizes in a dual fluidized bed pilot plant for biomass steam gasification,
828 Ind. Eng. Chem. Res. 51 (2012) 10492-10502.

829 [76] S. Kern, C. Pfeifer, H. Hofbauer, Gasification of lignite in a dual fluidized bed gasifier —
830 Influence of bed material particle size and the amount of steam, Fuel Process. Technol. 111
831 (2013) 1-13.

832 [77] G. Elordi, M. Olazar, P. Castaño, M. Artetxe, J. Bilbao, Polyethylene cracking on a spent
833 FCC catalyst in a conical spouted bed, Ind. Eng. Chem. Res. 51 (2012) 14008-14017.

834

835